Chemical Engineering Journal 288 (2016) 19–27

Contents lists available at ScienceDirect

Chemical Engineering Journal

journal homepage: www.elsevier.com/locate/cej

Hydrothermally-treated Na-X as efficient adsorbents for butadiene removal

Guillaume B. Baur [a], Florent Héroguel [b], Jonathan Spring [a], Jeremy S. Luterbacher [b], Lioubov Kiwi-Minsker [a,c,*]

[a] Group of Catalytic Reaction Engineering, Ecole Polytechnique Fédérale de Lausanne, Station 6, Lausanne CH-1015, Switzerland
[b] Laboratory of Sustainable and Catalytic Processing, Ecole Polytechnique Fédérale de Lausanne, Station 6, Lausanne CH-1015, Switzerland
[c] Regional Technological Centre, Tver State University, Tver 170100, Russian Federation

HIGHLIGHTS

- Hydrothermally treated industrial Na-X is highly efficient for butadiene adsorption.
- Hydrothermal treatment dealuminates the zeolite.
- New OH-groups are formed for adsorption of butadiene.
- Adsorption isotherms fit well the Dubinin–Astakhov model.
- Adsorption enthalpy of −45 kJ mol^{-1} was calculated.

GRAPHICAL ABSTRACT

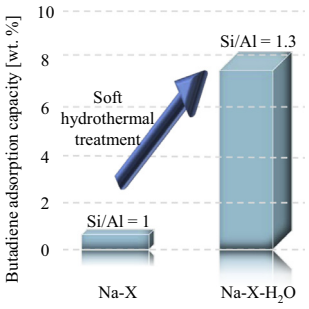

ARTICLE INFO

Article history:
Received 24 September 2015
Received in revised form 24 November 2015
Accepted 25 November 2015
Available online 30 November 2015

Keywords:
Butadiene adsorption
Na-X zeolite
Soft hydrothermal treatment
Dubinin–Astakhov adsorption isotherm
Butadiene adsorption enthalpy
TPD modeling

ABSTRACT

An efficient adsorbent for butadiene was synthesized via soft hydrothermal treatment (2 h in boiling water followed by 1 h calcination at 573 K) of industrial Na-X. The adsorption capacity of the zeolite was studied in the low concentration range (20–300 ppmv). Whereas original Na-X presents a very small adsorption, its treated counterpart shows a large capacity. The characterization of the zeolite suggests that the soft hydrothermal treatment dealuminates the zeolite leaving behind new OH-groups responsible for the adsorption of butadiene on the zeolite lattice. The adsorption isotherms were determined for the hydrothermally treated zeolites and the results were found to be consistent with the Dubinin–Astakhov (D–A) model. The adsorption enthalpy of butadiene on the treated Na-X was obtained from the D–A equation and from the modeling of temperature-programmed desorption profiles. Both methods gave a value of −45 kJ mol^{-1} suggesting chemical interactions of butadiene with the zeolite lattice. In summary, we report an efficient adsorbent for butadiene removal from diluted stream being valuable material for reducing butadiene emissions.

1. Introduction

Volatile organic compounds (VOC) are harmful and detrimental for human health and the environment even at low concentration. Therefore, their release in the atmosphere is subjected to legal limits [1,2] making VOC removal from industrial gas emissions of great importance during the last decades [3]. For gas mixture containing diluted VOC, adsorption is often the most efficient removal method [4]. It does not require any energy input and it can be applied for a wide variety of compounds. Besides zeolite and silica [5], activated carbon is the main adsorbent used for VOC abatement due to its large specific surface area, its network of

* Corresponding author at: Group of Catalytic Reaction Engineering, Ecole Polytechnique Fédérale de Lausanne, Station 6, Lausanne CH-1015, Switzerland. Tel.: +41 (0) 21 693 3182; fax: +41 (0) 21 693 3667.
E-mail address: lioubov.kiwi-minsker@epfl.ch (L. Kiwi-Minsker).

http://dx.doi.org/10.1016/j.cej.2015.11.096
1385-8947/

micropores and its versatility to different compounds [6]. Activated carbon is very efficient for high boiling point VOC such as benzene or toluene due to pore filling mechanisms [7], but its adsorption capacity towards low boiling point VOC is poor, particularly when used with diluted mixtures [8].

Efficient adsorption of low boiling point VOC from diluted mixtures requires specific adsorbate–adsorbent interactions [9,10]. Hence, functionalization of activated carbon surface by nanoparticles [11], liquid layer deposition [12] or creation of oxygen-containing groups [13] has been investigated. However, only a limited number of active sites can be formed. Zeolites are other valuable adsorbents because they can offer additional functional groups creating interactions with the adsorbate [14]. In addition, zeolites enable easy regeneration by calcination, which is incompatible with carbon.

Zeolites consist of crystalline microporous aluminosilicates with an infinite three dimensional framework of AlO_4 and SiO_4 [15]. They present an important pore volume and a large specific surface area, as well as surface acid sites, which are active in catalysis of multiple reactions [16,17]. In the context of adsorption, these acid sites can serve for specific VOC. Two types of acidity are usually reported for zeolites: Brønsted and Lewis [18]. Brønsted acid sites are formed by aluminum atoms connected to silicon by a "bridging hydroxyl" (Si–OH–Al) where the framework negative charge is compensated by a proton. Lewis acid sites are composed of aluminum or silicon atoms with low coordination [19] or of alkaline cations such as sodium [20]. Recently, reports have demonstrated that Brønsted sites could interact with the π bond of olefins in H-ZSM-5 [21].

The present study investigates butadiene adsorption over Na-X and water-treated Na-X zeolites. Butadiene whose emissions can come from gas exhaust of coal plants [22] is a low boiling point VOC (269 K) making its adsorption from diluted gas streams particularly challenging. Transition metal exchanged zeolites [23,24] or polycations metal exchanged zeolites [25] have been previously reported as good adsorbents for butadiene. The authors suggested that interactions between the *d* orbital of the transition metal and the electron rich π system of butadiene were responsible for its adsorption [26]. Although these exchanged zeolites were efficient adsorbents, the adsorption mechanism is still unclear. Moreover, since many transition metals are efficient for butadiene adsorption, the role of the exchanged metal is not clear [24].

The goal of the present study is to investigate butadiene adsorption on Na-X zeolites aiming at a development of an efficient adsorbent. Butadiene adsorption isotherms and temperature-programmed desorption (TPD) experiments were carried out to obtain the adsorption enthalpy. We found that a water-treated Na-X zeolite was an efficient adsorbent for butadiene and showed markedly superior performance as compared to its untreated form. To the best of our knowledge this is the first report of the effect of zeolite soft hydrothermal treatment for butadiene adsorption. The combination of surface sites characterization by Fourier-transformed infra-red (FTIR) and ^{27}Al magic angle spinning (MAS) nuclear magnetic resonance (NMR) spectroscopies, pyridine and ammonia TPD, isopropylamine temperature-programmed decomposition as well as *in situ* DRIFT suggested that Brønsted acid sites are mainly involved in the butadiene adsorption mechanism.

2. Experimental part

2.1. Material

The zeolites samples used in this study were prepared from commercial Na-X (Sigma–Aldrich, 13×, pellets 1.6 mm, Switzerland). The pellets were ground in a Fritsch centrifugal ball mill (Germany) at low rotation speed during 2 min. Milled Na-X pellets were then sieved in Fritsch Analysette (Germany) to obtain a pellet size fraction of 350–600 μm.

Na-X–H_2O was prepared by treatment of 1 g of Na-X with 100 ml of deionized water. The treatment was performed during 120 min in a beaker maintained at 373 K. Then the Na-X was filtered and dried to remove the excess of water. The adsorbent was placed in a quartz boat and heated in a horizontal quartz tube furnace up to 573 K at 10 K min^{-1} under 100 cm^3 min^{-1} in N_2 (>99.995%, Carbagas, Switzerland). It was then held at 573 K for 1 h. All chemicals mentioned below were purchased from Sigma–Aldrich (Switzerland) unless specified otherwise.

2.2. Adsorbent characterization

The specific surface area (SSA) and pore size distribution were determined by physical adsorption of N_2 at 77 K using a Sorptomatic 1990 (Carlo Erba Instruments). Prior to analysis, the samples were outgassed at 523 K for 2 h under vacuum ($7 \cdot 10^{-2}$ bar). N_2 adsorption/desorption isotherms were recorded at 77 K over the relative pressure range of $0.0005 \leqslant p/p_0 \leqslant 0.98$. The total pore volume and specific surface area were calculated using the BET method [27]. The BET equation was linearized in the 0.001–0.05 pressure range and the pore volume was calculated with the N_2 volume adsorbed at $p/p_0 = 0.98$.

Scanning electron microscopy (SEM) was carried out via a Carl Zeiss MERLIN FE-SEM equipped with two annular and Everhart–Thornley secondary-electron (SE) detectors operated at an accelerating voltage of 5–30 keV with a beam current of 1.0–3.0 nA. ZeissSmartSEM software was used for data acquisition/manipulation.

Powder X-ray diffractograms were recorded on a Bruker/Siemens D500 incident X-ray diffractometer using Cu Kα radiation. The samples were scanned at a rate of 0.02° step^{-1} over the range 5–40°. Diffractograms were identified by direct comparison with the JCPDS-ICDD reference standards, i.e. Na-X (045-0946).

The elemental composition of the zeolites was determined by atomic absorption spectroscopy (AAS) using a Shimadzu AA-6650 spectrometer with a flame supplied by an N_2O-acetylene mixture (for Si or Al) or an air–acetylene mixture (for Na). Prior to the measurements, the samples were dissolved in boiling aqua regia (1:3 v/v HNO_3/HCl) under reflux during 1 h followed by the addition of NH_4F.

^{27}Al MAS NMR spectroscopy was recorded on Bruker 800 MHz spectrometer with a conventional double resonance 2.5 mm CP-MAS probe. In all experiments, the rotation frequency was set to 15 kHz and the spectra were recorded at room temperature.

Infrared spectra were recorded on a Perkin Elmer Spectrum II equipped with a nitrogen cooled MCT detector. Samples were placed into the Harrick Ultra High Vacuum DRIFT cell where they could be heated under gas flow or vacuum with temperature. Typically, 24 scans were accumulated for each spectrum at a resolution of 4 cm^{-1}.

The adsorption of butadiene on zeolites was characterized by DRIFT measurement. Prior to adsorption measurement, the sample placed in a DRIFT cell described earlier was treated at 573 K in N_2 to perform partial dehydroxylation. The butadiene adsorption was carried out at room temperature.

Zeolite acid sites were characterized by pyridine adsorption–desorption. Qualitative data were obtained by FTIR analysis of adsorbed pyridine. The sample was placed in the DRIFT cell described above, treated at 373 K under N_2 flow for 1 h, cooled down to room temperature and contacted with a N_2 stream saturated with pyridine vapor. Flow was switched back to N_2 to remove physisorbed pyridine and the spectrum was recorded. Temperature was gradually increased and DRIFT spectra were recorded at chosen temperatures to characterize acid strength.

Quantitative data were obtained by pyridine TPD monitored by a thermal conductivity detector on a Micromeritics Autochem 2920 II instrument. Typically, 250 mg of sample were dried under

He flow at 773 K (10 K min^{-1}) for 1 h. After cooling down to 373 K, samples were saturated with 10 successive 0.5 cm^3 pulses of He stream (50 cm^3 min^{-1}) containing 0.1 bar of pyridine vapor using built-in vapor generator. Flow was switched to He and TPD was recorded from 373 to 773 K.

NH_3 TPD was recorded on a Micromeritics Autochem 2920 II instrument using MKS Cirrus 2 mass spectrometer. Typically, 250 mg of sample were pretreated under H_2 flow (50 cm^3 min^{-1}) at 643 K for 60 min and saturated with a 1% NH_3/He vol/vol mixture (50 cm^3 min^{-1}) at 393 K for 30 min. After flushing under He flow (50 cm^3 min^{-1}) for 60 min, mass 16 was monitored and temperature was increased to 773 K (10 K min^{-1}).

Isopropylamine TPD was performed on a Micromeritics Autochem 2920 II instrument using MKS Cirrus 2 mass spectrometer. Typically, 250 mg of sample were calcined *in situ* at 773 K, saturated at 473 K with 20 successive pulses (0.5 cm^3) of He stream (50 cm^3 min^{-1}) containing 0.1 bar of isopropylamine vapor using built-in vapor generator. After flushing under He flow (50 cm^3 min^{-1}) for 30 min, mass 41 was monitored and temperature was increased to 773 K (10 K min^{-1}).

2.3. Dynamic adsorption measurement

Before any measurements, the zeolite samples (40 ± 0.1 mg) were placed in the central part of a glass tubular reactor described elsewhere [10]. The samples were then outgassed at 298 K in a He flow (40 cm^3 min^{-1}). Standard adsorption experiments were carried out at 298 ± 1 K in a Carbolite MTF oven with a gas flow rate of 300 cm^3 min^{-1} (linear velocity – 0.5 m s^{-1}) regulated by mass flow controllers (EL-FLOW, Bronkhorst). The gaseous mixture used for adsorption experiments was obtained by diluting a 0.1% v/v butadiene mixture in He (Carbagas, Switzerland) 10 times with pure He (Carbagas). The diluted butadiene mixture (100 ppmv) was injected within the adsorbent bed. The outlet of the adsorbent bed was continuously monitored by a mass spectrometer (HPR 20, Hiden Analytical). The absence of channeling or of preferential path formation in the adsorbent bed was ensured by comparison to an argon (Ar 2% v/v in He) breakthrough signal measured in a separate experiment, for which a piston-type flow pattern was confirmed [10].

A standard adsorption capacity measurement consisted of the following steps:

1. Stabilization of butadiene mixture flow through the bypass for 15 min to measure the inlet butadiene concentration.
2. After switching the flow from the bypass to the reactor, the butadiene mixture flowed through the adsorbent bed until the continuously measured outlet butadiene concentration reached its inlet value, which was measured during the stabilization step.

This sequence allowed the recording of a breakthrough curve. The breakthrough curves were numerically integrated to calculate the adsorption capacities. Each experiment was carried out three times and mean values are reported herein.

Butadiene adsorption isotherms were obtained by varying the butadiene partial pressure (25–300 ppmv) and the adsorption temperature. Similarly to standard adsorption experiments, breakthrough curves were numerically integrated. Butadiene isotherms were numerically simulated using a theoretical model of adsorption. The parameters of the model were adjusted to get the best fit of the experimental data using the "fittype" function in Matlab.

2.4. Temperature-programmed desorption (TPD)

The TPD of butadiene was carried out in the same setup with the samples (40 ± 0.1 mg) saturated by butadiene (100 ppmv) at 298 K. The adsorbents were then heated in a He flow (100 cm^3 min^{-1}) at different temperature ramps (3–30 K min^{-1}). The outlet concentration of desorbed butadiene was continuously monitored by the mass spectrometer (mass 54) and plotted as a function of temperature to obtain a TPD pattern.

3. Results and discussion

3.1. Zeolite characterization

3.1.1. Morphology

The pellet size of about ca. 500 μm, which was selected to avoid the pressure drop encountered with small particles and mass transfer limitations appearing with large particles, was confirmed by SEM imaging (Fig. 1A). The pellets are constituted of elementary microcrystals of around 4–5 μm linked together (Fig. 1B). The appearance of the zeolite microcrystal was preserved after soft hydrothermal treatment as shown in Fig. 1C.

The N_2 adsorption isotherms of the Na-X before and after water treatment display similar features implying that the water treatment does not affect the porosity of the zeolite (Fig. 2). Both isotherms shows an increase of the N_2 adsorption capacity a low p/p_0 similarly to type I isotherm according to the IUPAC classification indicating a microporous material (pore diameter < 2 nm) [28]. The increase in adsorption capacity at $p/p_0 > 0.8$ likely corresponds to N_2 adsorption on the external surface of the zeolite due to its small crystals size (Fig. 1B and C). Hence the outer surface of zeolite crystals is of importance only at high adsorbate partial pressure. Since the adsorption of butadiene is studied at low partial pressure ($p/p_0 < 2 \cdot 10^{-4}$) this surface is not important for the total amount of butadiene removed. The adsorption and desorption branches of N_2 are overlapping insuring the absence of mesoporosity. Hence the zeolite surface is characterized by microporosity and macroporosity. The SSA and the pore volume are presented in Table 1. As can be seen the soft hydrothermal treatment does not modify the porosity of the zeolite since both pore volume and the SSA remain almost constant (within the experimental error). The values reported are in the same range as already published values [29]. The "C" value of the BET equation is a qualitative representation of the first layer adsorption energy. The high value measured here (~50,000) is indicative of a microporous structure with a narrow pore size corresponding to the theoretical faujasite channel size of 7.4 Å [15].

3.1.2. Bulk composition

XRD patterns of both Na-X and Na-X–H_2O display sharp peaks and match the faujasite pattern, confirming the original crystalline structure of the zeolite after water treatment (Fig. S.1).

The Si/Al and Na/Al ratios of both samples were measured by AAS elemental analysis (Table 1). A Na/Al ratio of 0.92 and 0.95 is obtained for Na-X and Na-X–H_2O, respectively, attesting that the majority of the framework counterions are sodium. The Si/Al ratio of the zeolite is slightly increased upon water treatment (1.3 for Na-X–H_2O vs 0.96 for Na-X). This partial zeolite dealumination that occurred during the water treatment could be attributed either to the removal of aluminum from the zeolite lattice or to the removal of extraframework aluminum cations.

^{27}Al MAS NMR spectra of Na-X and Na-X–H_2O displayed a sharp band at 64 ppm, consistent with the presence of tetrahedrally coordinated aluminum in the zeolite framework as charge was compensated by a Na cation (Fig. S.2). No additional peak was observed for the water modified zeolite, most likely because the low abundance and broadness of the modified aluminum sites.

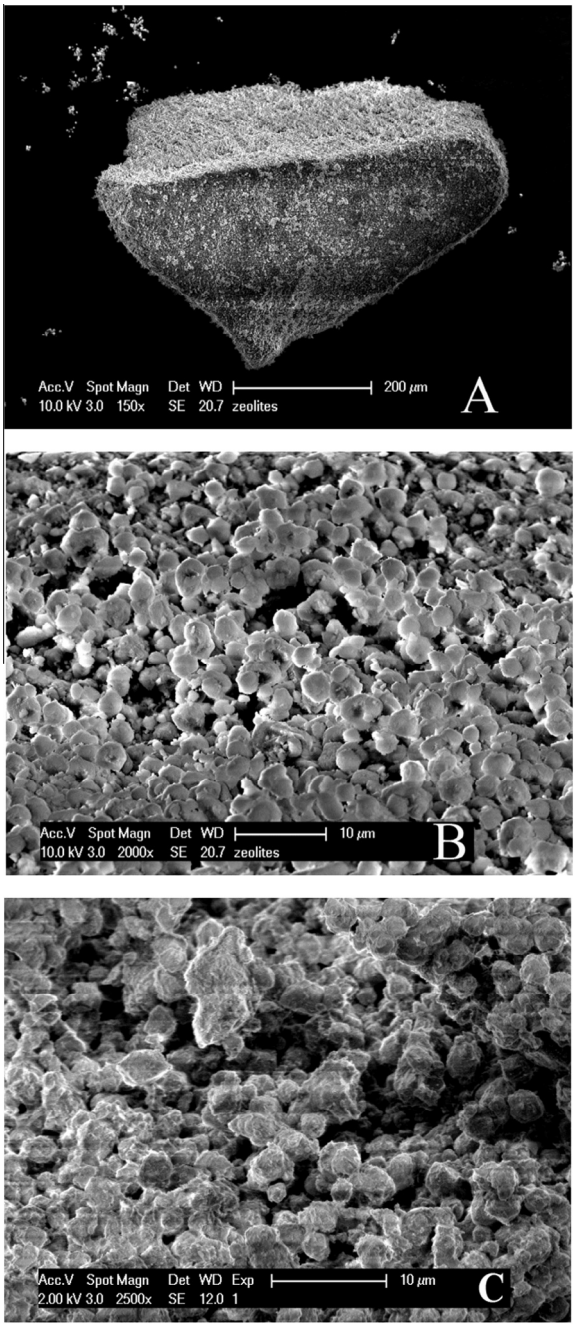

Fig. 1. SEM picture of original zeolite at different magnification, 150× (A) and 2000× (B) and after soft hydrothermal treatment (C).

3.1.3. Surface chemistry

The surface chemistry of the original and water treated zeolites was characterized by FTIR spectroscopy. Since zeolite surfaces are generally covered by chemi- and physi-sorbed water, samples were partially dehydroxylated under N_2 flow at 573 K in order to observe hydroxyl surface groups. Na-X displayed three distinct bands in the OH region (Fig. 3) at 3637 cm^{-1} (Si–OH–Al located in a large cavity) [30], 3700–3680 (–OH on extraframework/defect sites) [31,32] and 3734 cm^{-1} (silanols) [33]. A wide contribution is observed for Na-X between 3300 and 3500 cm^{-1}, attributed to the bonded OH partially located in small cavities.

Na-X–H_2O presents mainly bands at 3637 and 3734 cm^{-1} whereas the band at 3680 cm^{-1} observed for Na-X has a much lower intensity. Therefore, the water treatment most likely

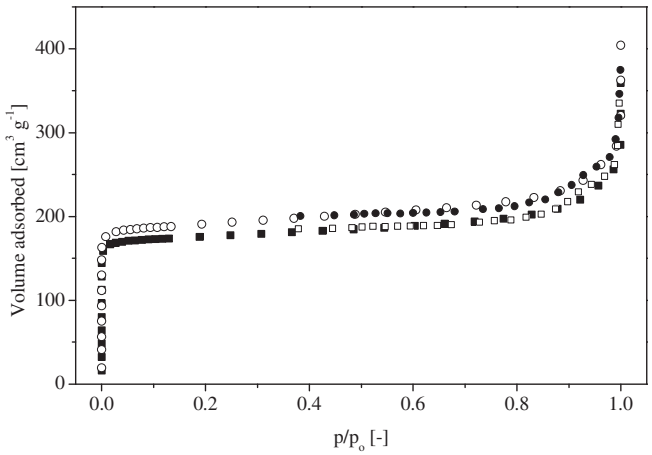

Fig. 2. N_2 adsorption isotherm of Na-X adsorption (○) and desorption (●) and Na-X–H_2O adsorption (■) and desorption (□).

Table 1
Elemental analysis of Na-X and Na-X–H_2O.

	Pore volume [$cm^3\ g^{-1}$]	SSA [$m^2\ g^{-1}$]	Si/Al	Na/Al
Na-X	0.31 ± 0.05	705 ± 50	0.96 ± 0.05	0.92 ± 0.05
Na-X–H_2O	0.34 ± 0.05	750 ± 50	1.3 ± 0.05	0.95 ± 0.05

resulted in the removal of Al (extraframework or Al within defect sites), leaving behind a big amount of Si–OH–Al located in large cavities (3637 cm^{-1}). This conclusion is in agreement with the increase of the Si/Al ratio from 0.96 to 1.3 measured by AAS.

Further FTIR analysis was carried out to probe the nature of surface acid sites using pyridine adsorption, the most common method for zeolite acid site characterization [34,35]. FTIR was recorded after contacting pyridine with zeolites at 323 K followed by treatment under vacuum at the same temperature for 30 min. The FTIR spectrum of Na-X only displayed the bands characteristic of pyridine bonded to Lewis acid sites at 1590, 1490 and 1443 cm^{-1} whereas H-bonded pyridine was not detected as shown by the absence of the band characteristic of Brønsted acid sites at 1541 cm^{-1} (Fig. 4) [36]. For Na-X–H_2O, Brønsted acid sites were detected with the characteristic band at 1541 cm^{-1} in addition to the 3 bands attributed to Lewis acid sites. The presence of Brønsted sites on Na-X–H_2O is due to a partial replacement of the

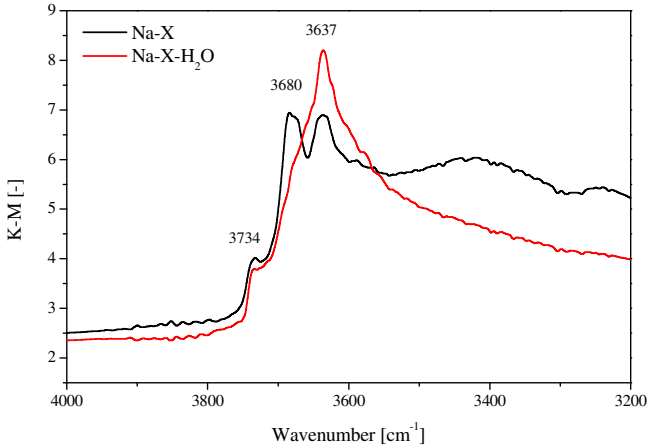

Fig. 3. OH region of FTIR spectra for Na-X and Na-X–H_2O (573 K).

extraframework Al^{3+} cations by H^+ cations upon water treatment. However, their content remains relatively low as compared to Lewis acid sites.

Quantitative analysis of zeolites surface acidity was carried out by pyridine temperature programmed desorption with a calibrated TCD. TPD profile of Na-X shows two types of acid sites: weak ones, identified by desorption peak at around 600 K and a strong one with a desorption peak at 740 K (Fig. 5). As shown by comparison of desorption signal areas, the quantity of weak acid sites was lower than the strong ones.

In contrast, the TPD profile of Na-X–H_2O did not display desorption peak at 600 K, indicating a disappearance of the weak acid sites upon water treatment. This type of weak acid sites was attributed to unsaturated atom in a defective zeolite framework [37], or extra framework $Al(OH)_3$ and $Al(OH)^{2+}$ [38,39]. However, since the TCD profile of Na-X–H_2O started to rise at around 650 K, one can suppose that a small amount of these sites still existed on the zeolite surface. These results confirm the hypothesis of the removal of extra-framework aluminum concomitant with the formation Si–OH–Al being consistent with the results of FTIR (Fig. 4) and elemental analysis (Table 1).

The numerical integration of the second desorption peak of pyridine (740 K) allows the calculation of total amount of strong acid sites. For Na-X and Na-X–H_2O similar value has been found with 0.16 and 0.15 mmol g^{-1}, respectively. Such value, far below the theoretical maximum value of acid sites reported for H-USY (3 mmol g^{-1}) [40], is explained by the Na^+ form of the zeolite.

Since the Brønsted acid sites seems to play an important role in the butadiene adsorption mechanism, the relative abundance of Brønsted acid sites for both materials was determined by temperature-programmed decomposition of isopropylamine (Fig. 6) monitored by a mass spectrometer. Isopropylamine reacts selectively with Brønsted acid sites to produce propylene and ammonia via a mechanism similar to the Hofmann elimination [41]. Propylene production profiles showed that Brønsted acid sites were more abundant on Na-X–H_2O surface as compared to Na-X. The creation of Brønsted acid sites is likely occurring via an exchange of Na^+ ions with H^+ ions during the soft hydrothermal treatment. Hence strong acidity is constant in both zeolites as shown by pyridine TPD (Fig. 5). In the case of Na-X we suggest that Lewis sites and Brønsted acid sites are contributing to the strong acidity since both type of sites were detected. The soft hydrothermal treatment is suggested to create Brønsted acid sites from Lewis acid sites explaining the larger amount of Brønsted acid sites in Na-X–H_2O (Fig. 6).

Finally, ammonia TPD was performed giving identical total amounts of acid sites for both materials (0.8 mmol g^{-1}). Since ammonia is a strong base and a small molecule, the measured number of acid sites included both weak acid sites as well as sites located in cavities, which might not play a role in butadiene adsorption (Fig. S.3). The higher amount of acid sites measured using ammonia as compared to pyridine is attributed to a weaker basicity of the latter (pKb of 9 and 5 for pyridine and ammonia, respectively) [42]. Hence, while both basic probes react with strong acid sites, weak acid sites are only titrated using ammonia. In addition, the smaller sterical hindrance of ammonia as compared to pyridine can allow access of ammonia to acid sites located onto cavities, whereas such sites are not accessible to pyridine.

In summary, the main characteristics caused by the soft hydrothermal treatment of Na-X were: (i) partial zeolite dealumination with the removal of extraframework Al species; (ii) increase of the amount of Brønsted acid sites; (iii) conservation of the zeolite framework crystallinity with a small increase of pore volume and preservation of the mean pore diameter.

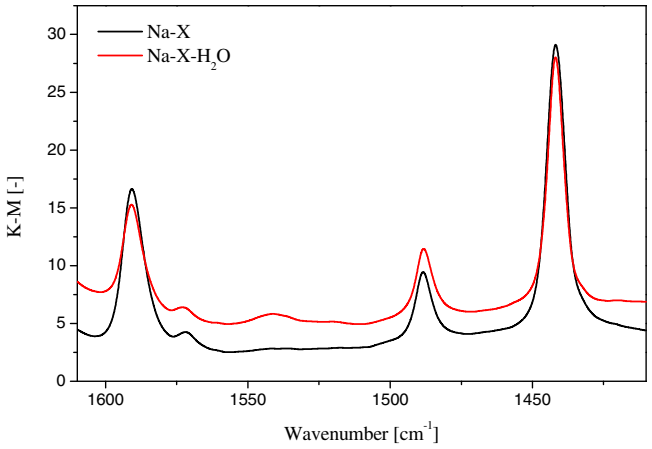

Fig. 4. FTIR spectra of pyridine adsorption on Na-X and Na-X-H_2O.

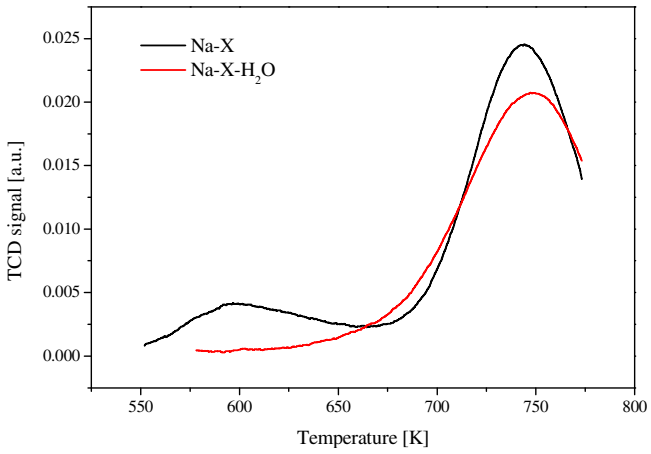

Fig. 5. TPD spectra of pyridine of Na-X and Na-X–H_2O.

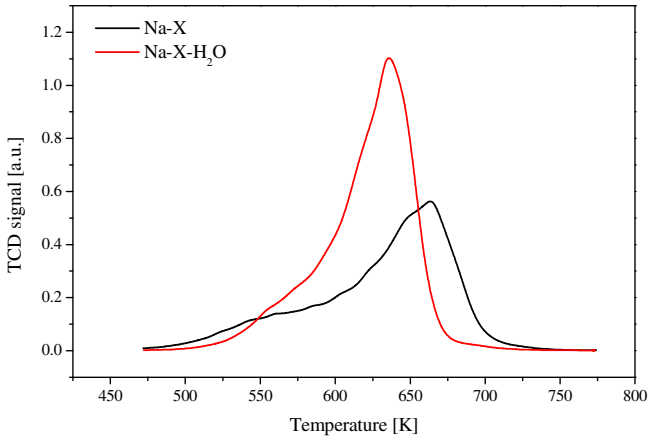

Fig. 6. Propylene profiles during temperature programmed decomposition of isopropylamine with zeolites Brønsted acid sites.

3.2. Butadiene adsorption

Adsorption of butadiene (100 ppmv) was performed over Na-X and Na-X–H_2O. Adsorption capacity was calculated by integration of the area defined by the butadiene and the argon breakthrough curves (Fig. 7). Adsorption capacity of the original Na-X was close to zero whereas it reached 7.2 wt.% for Na-X–H_2O. The butadiene outlet concentration remained zero for around 20 min with Na-

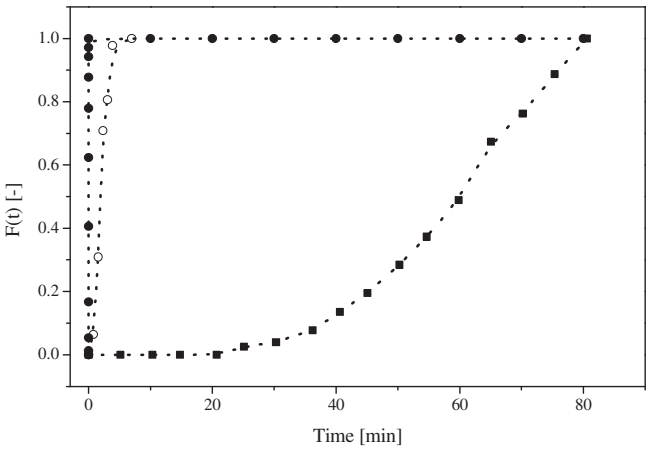

Fig. 7. Butadiene (100 ppmv) breakthrough curves of Na-X (○), Na-X-H_2O (■) and 2% (v/v) argon tracer (●) at 298 K and 300 cm^3 min^{-1}.

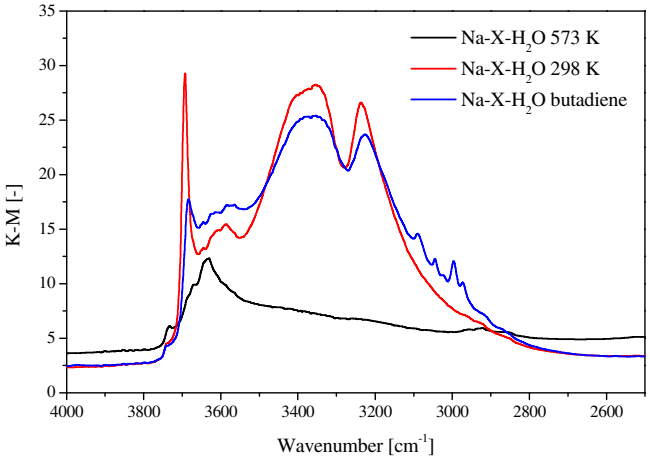

Fig. 8. IR spectra of *in situ* butadiene adsorption on Na-X–H_2O.

X–H_2O indicating total butadiene removal. Hence, the material obtained after water treatment was an efficient adsorbent for butadiene.

In order to gain insight into the butadiene adsorption mechanism, adsorption was monitored by *in situ* FTIR spectroscopy (Figs. 8 and 9). Upon cooling down to room temperature, the recorded spectrum displayed an increase of the 3000–3500 cm^{-1} broad bands for both Na-X and Na-X–H_2O due to the partial rehydroxylation by the traces of moisture present in the N_2 gas flow. The sharp band appearing at 3693 cm^{-1} upon cooling the sample was attributed to the rehydroxylation of the remaining extraframework Al sites.

After exposure of Na-X–H_2O to butadiene at 298 K, the latter band at 3693 cm^{-1} suddenly decreased. Simultaneously, C–H bands appeared around 3000 cm^{-1}, indicating butadiene adsorption and revealing an interaction of butadiene with the zeolite surface (Fig. 8). In contrast, exposure of Na-X to butadiene led to a very slight adsorption (Fig. 9) without a decrease of the 3693 cm^{-1} band. Instead, a constant rehydroxylation due to moisture present in the butadiene flow was observed with the increase in intensity of the 3693 cm^{-1} band and the 3400 cm^{-1} shoulder. Such observation indicates that the OH band at 3693 cm^{-1} (characteristic of extraframework Al sites) was not involved in the butadiene adsorption. This is in line with previous reports which had suggested that interactions of olefin bonds with Brønsted acid sites (Si–OH–Al) are the only responsible for adsorption [21,43,44]. It

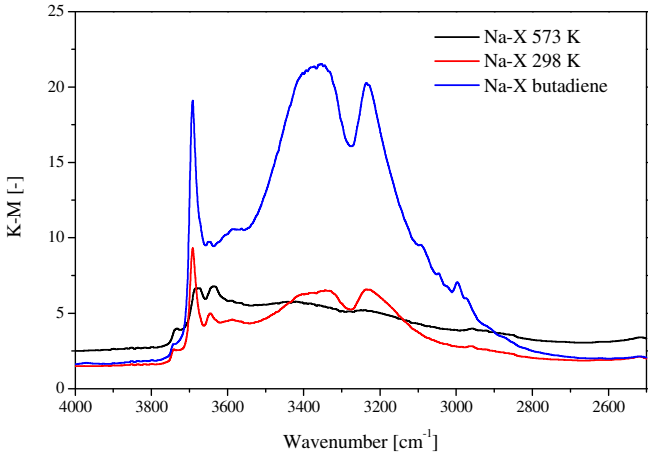

Fig. 9. IR spectra of *in situ* butadiene adsorption on Na-X.

seems to be a reason for low adsorption of butadiene in Na-X since only a very small amount of Brønsted sites were detected.

Therefore, we suggest that a high amount of extraframework Al prevented interactions between butadiene and the zeolite surface. Consequently, the removal of these Al species leaving behind a big amount of Si-OH-Al located in a large cavity considerably increased (25-fold) the zeolite adsorption capacity. However, a slight dealumination of the zeolite framework may also take place during soft hydrothermal treatment of zeolites.

In summary, dealumination is forming a favorable zeolite morphology and surface chemistry allowing efficient butadiene adsorption. Such behavior is observed for Na-X–H_2O where extra-framework Al have been removed leaving a favorable surface for butadiene. On the contrary the presence of a large amount of extra-framework Al in Na-X prevents the adsorption of butadiene.

3.3. Butadiene isotherms

Butadiene adsorption isotherms over Na-X–H_2O were measured to gain a deeper insight into the adsorption mechanism. By varying butadiene concentration (25–300 ppmv) and temperature of adsorption (298–333 K), a set of adsorption isotherms was obtained for Na-X–H_2O. Since it is particularly adapted for microporous material, the Dubinin–Astakhov (D–A) model, which is a generalization of the Dubinin–Radushkevich model, was used to fit the experimental data [45,46]. The D–A equation takes the following form:

$$W = W_0 \exp\left(-\left(\frac{A}{\beta E_0}\right)^n\right) \quad (1)$$

The model variables are: the adsorbed volume (W), the maximum adsorbed volume (W_0) expressed in cm^3 g^{-1} and the characteristic adsorption energy (E_0) expressed in kJ mol^{-1}. The parameter n represents the heterogeneity of the adsorbent surface and is linked to the pore size distribution. The parameter β is a constant that depends on the nature of the adsorbate called the affinity coefficient. A value of 0.97 was obtained for butadiene using the molar volume prediction [47]. The parameter A represents the Polanyi adsorption potential and is equal to the difference between the chemical potential of the adsorbate in the liquid state and in the adsorbed state at the same temperature.

$$A = RT \ln\left(\frac{p_0}{p}\right) \quad (2)$$

where p_0 is the vapor pressure, p is the adsorbate partial pressure and T is the temperature at which the adsorption experiment took

place. In this model the adsorbed phase is supposed to be liquid. For sake of simplicity, the maximum adsorbed volume ($cm^3\ g^{-1}$) is expressed as the saturation capacity ($mol\ kg^{-1}$) using the liquid molar volume. The variation of the liquid molar volume with temperature is taken into account by using the thermal expansion coefficient of the saturation capacity (δ). This parameter has been fixed to 0.001 [K^{-1}] [48].

The isosteric heat of adsorption can be calculated by combining the D–A model with the Van't Hoff and the Clausius–Clapeyron equations [48].

$$-\Delta H = \Delta H_{vap} + \beta E_0 \left(\ln\left(\frac{1}{\theta}\right)\right)^{1/n} + \frac{\beta E_0 \delta T}{n}\left(\ln\left(\frac{1}{\theta}\right)\right)^{-1/n} \quad (3)$$

with

$$\theta = \frac{q}{q_{max}} \quad (4)$$

where ΔH_{vap} is the heat of vaporization, which for butadiene has been reported as $-22.7\ kJ\ mol^{-1}$ [49] and q is the adsorbed quantity.

The isosteric adsorption enthalpy depends on the characteristic adsorption energy (E_0) and on the adsorbent loading (θ). The maximum adsorption capacity and the characteristic adsorption energy were obtained by fitting the experimental data to Eq. (1) for all the isotherms as shown in Fig. 10.

We systematically obtained a good fit of the experimental data with the D–A equation as the curve determination coefficient (R^2) was always larger than 0.97. The parameters (E_0, W_0 and n) used to fit the experimental points are presented in Table 2. The model predicted a maximum adsorption capacity of $2.05\ mol\ kg^{-1}$ at 298 K. Therefore, already at 300 ppmv a theoretical fractional loading close to 0.8 was obtained, which is indicative of the efficiency of Na-X–H_2O zeolite for butadiene adsorption from diluted stream. Adsorption of 2.05 mol of butadiene per kilo of adsorbent represents a volume of $0.17\ cm^3\ g^{-1}$ whereas the total pore volume calculated from the BET equation was around $0.28\ cm^3\ g^{-1}$. The difference between the maximum adsorption capacity calculated with butadiene adsorption and the N_2 adsorption isotherm can be explained by the nature of the D–A equation. Since this equation considers only the filling of micropores, the potential adsorption of butadiene on the zeolite outer surface is not taken into account, whereas it volume was accounted in the volume calculated from the N_2 adsorption isotherm. A zeolite microporous volume of $0.19\ cm^3\ g^{-1}$ was calculated at $p/p_0 = 0.2$. At saturation, butadiene was thus almost entirely filling the zeolite cavities.

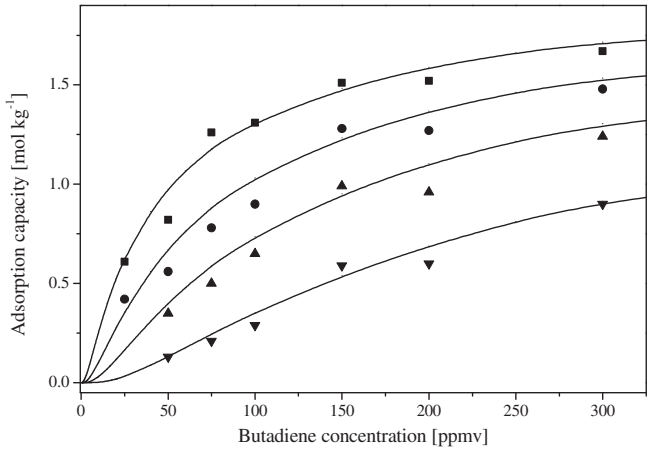

Fig. 10. Butadiene adsorption isotherm on Na-X–H_2O fitted with the D-A model at different temperature: 298 K (■), 308 K (●), 318 K (▲), 333 K (▼).

Table 2
Parameters of the D–A equation for butadiene adsorption on Na-X–H_2O.

	W_0 [$cm^3\ g^{-1}$]	E_0 [$kJ\ mol^{-1}$]	n
Na-X–H_2O	0.17 ± 0.05	22 ± 4	6 ± 0.05

Therefore, the modification of Na-X by soft hydrothermal treatment likely occurred uniformly through the whole zeolite framework allowing an almost complete micropore filling by butadiene in Na-X–H_2O under saturation conditions. We propose that this pore filling was enabled in Na-X–H_2O due to a more favorable surface chemistry obtained by the partial dealumination of the zeolite.

The relatively large n value obtained for the fitting of the D–A equation to the experimental data (Table 2) indicates homogeneity of the micropore sizes. Indeed, the exponent of the D–A equation is qualitatively indicative of the pore size heterogeneity. Low n values (1), (2) are generally obtained when fitting non-homogeneous microporous adsorbents [45,50] whereas n values comprised between 4 and 6 are commonly found for small and homogenous micropores such as zeolites [51].

The energetic parameter of the D–A equation (E_0) was estimated to be $22 \pm 4\ kJ\ mol^{-1}$ indicating a moderate adsorption strength due to the high volatility of butadiene. For comparison hexane has a characteristic adsorption energy of $30\ kJ\ mol^{-1}$ on carbon molecular sieve whereas it is only $17\ kJ\ mol^{-1}$ for ethane on the same adsorbent [52].

The isosteric enthalpy of adsorption was calculated using Eq. (3) and the parameters obtained from Eq. (1). The adsorption enthalpy was obtained by a summation of the vaporization enthalpy, the energetic parameter (E_0) and the change of the maximum capacity variation with temperature. An adsorption enthalpy value of $-45 \pm 4\ kJ\ mol^{-1}$ was obtained for a fractional loading of 0.63. Since the zeolite pores are homogeneous in size, the influence of the fractional loading on the enthalpy of adsorption was extremely small ($\sim 5\ kJ\ mol^{-1}$). For comparison, Eder and Lercher reported a slightly lower value for butane adsorption on Na-X ($-34\ kJ\ mol^{-1}$) [53] whereas $-50\ kJ\ mol^{-1}$ was reported on silicalite [54]. The enthalpy of adsorption of 1-butene was determined by numerical simulation being $-48\ kJ\ mol^{-1}$ [44], which was in the same range as the adsorption enthalpy for butadiene on Na-X–H_2O validating the adsorption model applied.

3.4. Temperature-programmed desorption

The interaction between butadiene and the active adsorption sites was characterized by TPD, allowing quantifying the adsorption energy. It can be considered as a complementary method to the adsorption isotherm. Desorption of butadiene from Na-X–H_2O was studied at different temperature ramps.

The experiment was carried out by monitoring mass 54 corresponding to the molecular ion of butadiene at the reactor outlet. TPD profiles showed only one desorption peak signifying that one type of adsorption site is present in the zeolite network (Fig. 11). The integration of the butadiene desorption curve revealed that not all the adsorbed butadiene could be desorbed. The mass balance was systematically smaller than 1. The incomplete desorption of butadiene was confirmed by a set of adsorption–desorption cycles where a systematic decrease of the adsorption capacity was observed. Since zeolite is known to act as a cracking catalyst at high temperature we screened for other desorbed species by varying the detected mass with the mass spectrometer however only butadiene could be detected. This phenomenon suggested that a heavy compound such as an oligomer or polymer was formed in the zeolite either during the adsorption process or at higher temperature during the TPD.

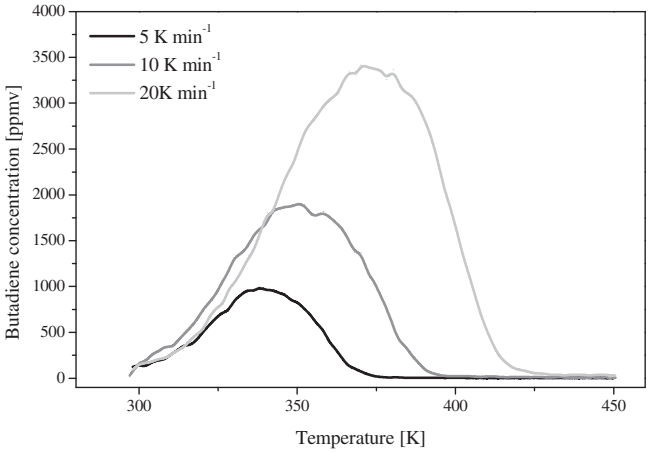

Fig. 11. TPD profiles: desorption of butadiene from Na-X–H_2O at different temperature ramp (100 cm^3 min^{-1} in He).

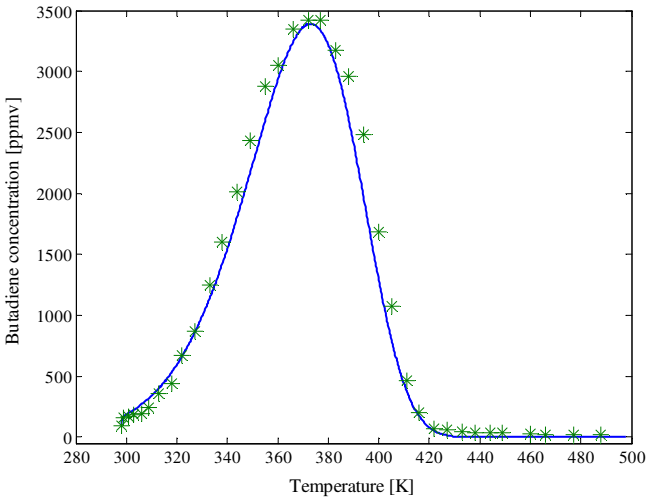

Fig. 12. Simulation of butadiene TPD pattern on Na-X–H_2O (20 K min^{-1}, 100 cm^3 min^{-1}).

The increase of the temperature ramps shifted the maximum desorption rate to higher temperatures. The kinetic desorption parameters – the activation energy of desorption (E_d) and the kinetic constant (k) – were obtained by parameter estimation of butadiene desorption. These two parameters were varied to obtain the best fit to the experimental points. The simulations were performed at different temperature ramps. Since in TPD experiment the temperature increases linearly, the desorption rate changes throughout the experiment. By solving the mass balance and the temperature variation equations simultaneously, a desorption curve was obtained. The development of the equation used to simulate desorption curves is presented elsewhere [55]. The gas phase concentration of desorbed species as a function of temperature was then obtained. An example is shown in Fig. 12.

The activation energy of desorption (E_d) obtained for the butadiene-zeolite system was constant for all the simulations performed. Since the model applied assumed a 1st order desorption kinetic, we suggest that the desorption kinetic of butadiene on Na-X–H_2O zeolites are indeed at the 1st order. The model gives an activation energy of desorption of 47.5 ± 2 kJ mol^{-1}, which, given that the activation energy of adsorption is negligible, can be used as a first approximation for the heat of adsorption (ΔH_{ad}) [56].

Mass transfer effects that have been reported in certain cases for large adsorbate quantities [55] are apparently avoided since a good fitting of the desorption model to the experimental data was observed. The value of the adsorption enthalpy was very close to the value determined by modeling of adsorption isotherms. Moreover, they were very close to the adsorption enthalpy reported for 1-butene, a very similar molecule [44]. The interactions created between the zeolite active site and butadiene together with the narrow microporosity of the zeolite network was likely to be responsible for strong butadiene adsorption. The porosity itself was not sufficient to have a large adsorption capacity since the original Na-X showed extremely limited butadiene removal from diluted streams.

4. Conclusions

We report that a simple soft hydrothermal treatment (2 h in boiling water followed by 1 h calcination at 573 K) of industrial Na-X zeolite considerably increases (25-fold) its adsorption capacity towards butadiene. In fact, while the original Na-X zeolite almost did not adsorb butadiene, Na-X–H_2O was highly efficient (7.2 wt.%) which is of great interest in view of VOC emission control.

The two zeolite materials were characterized in detail to gain insight into the adsorption mechanism. Bulk characterization revealed dealumination upon soft hydrothermal treatment of Na-X whereas surface characterization by FTIR and pyridine TPD showed the removal of extraframework Al species with concomitant formation of big amount of Si–OH–Al. The study by *in situ* FTIR spectroscopy further suggested that the presence of extraframework Al species on the zeolite surface prevented butadiene adsorption. The partial dealumination forming a favorable zeolite morphology and surface chemistry allowed efficient butadiene adsorption from diluted stream.

A set of butadiene adsorption isotherms was recorded and modeled with the Dubinin–Astakhov equation allowing to calculate the adsorption enthalpy. The value (−45 kJ mol^{-1}) was in the range reported for 1-butene adsorption on zeolites. To further confirm these results, butadiene TPD experiments were performed and fitted with TPD simulations providing a second independent adsorption enthalpy calculation. A similar value of the adsorption enthalpy was found confirming the consistency of the results.

In summary, soft hydrothermal treatment of industrial Na-X zeolite renders an efficient adsorbent for the removal of butadiene (low-boiling point VOC), which is of prime interest for atmospheric pollution control.

Acknowledgements

The authors highly appreciate the help of Oliver Beswick and Wiktor Bourée from EPFL for the SEM pictures.

The Russian Science Foundation (Grant 15-19-20023), Phillip Morris International and EPFL are acknowledged for funding.

Appendix A. Supplementary data

Supplementary data associated with this article can be found, in the online version, at http://dx.doi.org/10.1016/j.cej.2015.11.096.

References

[1] S.D. Piccot, J.J. Watson, J.W. Jones, A global inventory of volatile organic-compound emissions from anthropogenic sources, J. Geophys. Res. Atmos. 97 (1992) 9897–9912.

[2] C.F. Wu, S.Y. Wu, Y.H. Wu, A.C. Cullen, T.V. Larson, J. Williamson, L.J.S. Liu, Cancer risk assessment of selected hazardous air pollutants in Seattle, Environ. Int. 35 (2009) 516–522.

[3] G.R. Parmar, N.N. Rao, Emerging control technologies for volatile organic compounds, Crit. Rev. Environ. Sci. Technol. 39 (2009) 41–78.
[4] M.A. Lillo-Rodenas, D. Cazorla-Amoros, A. Linares-Solano, Behaviour of activated carbons with different pore size distributions and surface oxygen groups for benzene and toluene adsorption at low concentrations, Carbon 43 (2005) 1758–1767.
[5] X.S. Zhao, Q. Ma, G.Q. Lu, V.O.C. Removal, Comparison of MCM-41 with hydrophobic zeolites and activated carbon, Energy Fuels 12 (1998) 1051–1054.
[6] K.L. Foster, R.G. Fuerman, J. Economy, S.M. Larson, M.J. Rood, Adsorption characteristics of trace volatile organic-compounds in gas streams onto activated carbon-fibers, Chem. Mater. 4 (1992) 1068–1073.
[7] M.A. Lillo-Rodenas, D. Cazorla-Amoros, A. Linares-Solano, Benzene and toluene adsorption at low concentration on activated carbon fibres, Adsorpt. J. Int. Adsorpt. Soc. 17 (2011) 473–481.
[8] J.J. Pei, J.S.S. Zhang, On the performance and mechanisms of formaldehyde removal by chemi-sorbents, Chem. Eng. J. 167 (2011) 59–66.
[9] Y. El-Sayed, T.J. Bandosz, Acetaldehyde adsorption on nitrogen-containing activated carbons, Langmuir 18 (2002) 3213–3218.
[10] G.B. Baur, O. Beswick, J. Spring, I. Yuranov, L. Kiwi-Minsker, Activated carbon fibers for efficient VOC removal from diluted streams: the role of surface functionalities, Adsorpt. J. Int. Adsorpt. Soc. 21 (2015) 255–264.
[11] G.B. Baur, I. Yuranov, L. Kiwi-Minsker, Activated carbon fibers modified by metal oxide as effective structured adsorbents for acetaldehyde, Catal. Today 249 (2015) 252–258.
[12] C.J. Ma, X.H. Li, T.L. Zhu, Removal of low-concentration formaldehyde in air by adsorption on activated carbon modified by hexamethylene diamine, Carbon 49 (2011) 2873–2875.
[13] J.L. Figueiredo, M.F.R. Pereira, M.M.A. Freitas, J.J.M. Orfao, Modification of the surface chemistry of activated carbons, Carbon 37 (1999) 1379–1389.
[14] J. Pires, A. Carvalho, M.B. de Carvalho, Adsorption of volatile organic compounds in Y zeolites and pillared clays, Microporous Mesoporous Mater. 43 (2001) 277–287.
[15] C. Baerlocher, L.B. McCusker, W.M. Meier, B. Olson, ebrary Inc., International Zeolite Association. Structure Commission, Atlas of zeolite framework types, in: Published on behalf of the Structure Commission of the International Zeolite Association by Elsevier, Boston, Amsterdam, 2007.
[16] D. Barthomeuf, Zeolite acidity dependence on structure and chemical environment – correlations with catalysis, Mater. Chem. Phys. 17 (1987) 49–71.
[17] A. Corma, State of the art and future challenges of zeolites as catalysts, J. Catal. 216 (2003) 298–312.
[18] N. Katada, H. Igi, J.H. Kim, M. Niwa, Determination of the acidic properties of zeolite by theoretical analysis of temperature-programmed desorption of ammonia based on adsorption equilibrium, J. Phys. Chem. B 101 (1997) 5969–5977.
[19] L. Rodriguez-Gonzalez, F. Hermes, M. Bertmer, E. Rodriguez-Castellon, A. Jimenez-Lopez, U. Simon, The acid properties of H-ZSM-5 as studied by NH3-TPD and Al-27-MAS-NMR spectroscopy, Appl. Catal. A Gen. 328 (2007) 174–182.
[20] B.L. Su, D. Barthomeuf, Comparison of acid–base properties of FAU, EMT, LTL and MOR (Na forms) in benzene adsorption and alkylation of aniline with methanol, Appl. Catal. A Gen. 124 (1995) 81–90.
[21] J.N. Kondo, K. Domen, IR observation of adsorption and reactions of olefins on H-form zeolites, J. Mol. Catal. A Chem. 199 (2003) 27–38.
[22] Y. Liu, M. Shao, L. Fu, S. Lu, L. Zeng, D. Tang, Source profiles of volatile organic compounds (VOCs) measured in China: Part I, Atmos. Environ. 42 (2008) 6247–6260.
[23] A. Takahashi, R.T. Yang, C.L. Munson, D. Chinn, Cu(I)-Y-zeolite as a superior adsorbent for diene/olefin separation, Langmuir 17 (2001) 8405–8413.
[24] A. Takahashi, R.T. Yang, C.L. Munson, D. Chinn, Influence of Ag content and H_2S exposure on 1,3-butadiene/1-butene adsorption by Ag ion-exchanged Y-zeolites (Ag-Y), Ind. Eng. Chem. Res. 40 (2001) 3979–3988.
[25] A.M. Tsybulevski, L.M. Kustov, K.C. Weston, A.A. Greish, O.P. Tkachenko, A.V. Kucherov, 1,3-Butadiene adsorption over transition metal polycation exchanged faujasites, Ind. Eng. Chem. Res. 51 (2012) 7073–7080.
[26] R.T. Yang, A.J. Hernandez-Maldonado, F.H. Yang, Desulfurization of transportation fuels with zeolites under ambient conditions, Science 301 (2003) 79–81.
[27] S. Brunauer, P.H. Emmett, E. Teller, Adsorption of gases in multimolecular layers, J. Am. Chem. Soc. 60 (1938) 309–319.
[28] K.S.W. Sing, D.H. Everett, R.A.W. Haul, L. Moscou, R.A. Pierotti, J. Rouquerol, T. Siemieniewska, Reporting physisorption data for gas solid systems with special reference to the determination of surface-area and porosity (recommendations 1984), Pure Appl. Chem. 57 (1985) (1984) 603–619.
[29] X. Du, E. Wu, Porosity of microporous zeolites A, X and ZSM-5 studied by small angle X-ray scattering and nitrogen adsorption, J. Phys. Chem. Solids 68 (2007) 1692–1699.
[30] J. Datka, B. Gil, P. Baran, IR study of heterogeneity of OH groups in zeolite HY-splitting of OH and OD bands, J. Mol. Struct. 645 (2003) 45–49.
[31] A. Maijanen, E.G. Derouane, J.B. Nagy, FT-IR and solid-state NMR investigation of surface hydroxyl groups on dealuminated ZSM-5, Appl. Surf. Sci. 75 (1994) 204–212.
[32] M. Bevilacqua, T. Montanari, E. Finocchio, G. Busca, Are the active sites of protonic zeolites generated by the cavities?, Catal Today 116 (2006) 132–142.
[33] A. Janin, M. Maache, J.C. Lavalley, J.F. Joly, F. Raatz, N. Szydlowski, FT i.r. study of the silanol groups in dealuminated HY zeolites: Nature of the extraframework debris, Zeolites 11 (1991) 391–396.
[34] J.C. Lavalley, Infrared spectrometric studies of the surface basicity of metal oxides and zeolites using adsorbed probe molecules, Catal. Today 27 (1996) 377–401.
[35] S. Khabtou, T. Chevreau, J.C. Lavalley, Quantitative infrared study of the distinct acidic hydroxyl groups contained in modified Y zeolites, Microporous Mater. 3 (1994) 133–148.
[36] T. Barzetti, E. Selli, D. Moscotti, L. Forni, Pyridine and ammonia as probes for FTIR analysis of solid acid catalysts, J. Chem. Soc. Faraday Trans. 92 (1996) 1401–1407.
[37] F. Lonyi, J. Valyon, A TPD and IR study of the surface species formed from ammonia on zeolite H-ZSM-5, H-mordenite and H-beta, Thermochim. Acta 373 (2001) 53–57.
[38] S.H. Li, A.M. Zheng, Y.C. Su, H.L. Zhang, L. Chen, J. Yang, C.H. Ye, F. Deng, Bronsted/Lewis acid synergy in dealuminated HY zeolite: a combined solid-state NMR and theoretical calculation study, J. Am. Chem. Soc. 129 (2007) 11161–11171.
[39] G.L. Woolery, G.H. Kuehl, H.C. Timken, A.W. Chester, J.C. Vartuli, On the nature of framework Bronsted and Lewis acid sites in ZSM-5, Zeolites 19 (1997) 288–296.
[40] B. Louis, S. Walspurger, J. Sommer, Quantitative determination of Bronsted acid sites on zeolites: a new approach towards the chemical composition of zeolites, Catal. Lett. 93 (2004) 81–84.
[41] T.J.G. Kofke, R.J. Gorte, G.T. Kokotailo, W.E. Farneth, Stoichiometric adsorption complexes in H-ZSM-5, H-ZSM-12, and H-mordenite zeolites, J. Catal. 115 (1989) 265–272.
[42] E.P. Parry, An infrared study of pyridine adsorbed on acidic solids characterization of surface acidity, J. Catal. 2 (1963) 371–379.
[43] R.J. Gorte, D. White, Interactions of chemical species with acid sites in zeolites, Top. Catal. 4 (1997) 57–69.
[44] S. Jakobtorweihen, N. Hansen, F.J. Keil, Molecular simulation of alkene adsorption in zeolites, Mol. Phys. 103 (2005) 471–489.
[45] M.M. Dubinin, H.F. Stoeckli, Homogeneous and heterogeneous micropore structures in carbonaceous adsorbents, J. Colloid Interface Sci. 75 (1980) 34–42.
[46] M.M. Dubinin, Adsorption in micropores, J. Colloid Interface Sci. 23 (1967) 487–499.
[47] J.F. Wu, M.E. Stromqvist, O. Claesson, I.E. Fangmark, L.G. Hammarstrom, A systematic approach for modelling the affinity coefficient in the Dubinin–Radushkevich equation, Carbon 40 (2002) 2587–2596.
[48] D.D. Duong, Adsorption Analysis: Equilibria and Kinetics, Imperial College Press, London, UK, 1998.
[49] V. Majer, V. Svoboda, Enthalpies of vaporization of organic compounds: a critical review and data compilation, in: IUPAC Chemical Data Series No. 32, Blackwell Scientific Publ, Oxford, Boston etc., 1985, p. 300.
[50] M.M. Dubinin, Fundamentals of the theory of adsorption in micropores of carbon adsorbents – characteristics of their adsorption properties and microporous structures, Carbon 27 (1989) 457–467.
[51] N.D. Hutson, R.T. Yang, Theoretical basis for the Dubinin–Radushkevich (D–R) adsorption isotherm equation, Adsorpt. J. Int. Adsorpt. Soc. 3 (1997) 189–195.
[52] G.O. Wood, Affinity coefficients of the Polanyi/Dubinin adsorption isotherm equations – a review with compilations and correlations, Carbon 39 (2001) 343–356.
[53] F. Eder, J.A. Lercher, Alkane sorption in molecular sieves: the contribution of ordering, intermolecular interactions, and sorption on Bronsted acid sites, Zeolites 18 (1997) 75–81.
[54] T.J.H. Vlugt, R. Krishna, B. Smit, Molecular simulations of adsorption isotherms for linear and branched alkanes and their mixtures in silicalite, J. Phys. Chem. B 103 (1999) 1102–1118.
[55] G. Baur, I. Yuranov, A. Renken, L. Kiwi-Minsker, Activated carbon fibers for efficient VOC removal from diluted streams: the role of surface morphology, Adsorpt. J. Int. Adsorpt. Soc. 21 (2015) 479–488.
[56] R.J. Cvetanović, Y. Amenomiya, Application of a temperature-programmed desorption technique to catalyst studies, in: H.P.D.D. Eley, B.W. Paul (Eds.), Advances in Catalysis, Academic Press, 1967, pp. 103–149.